Optimization of High-Speed WIG Airfoil with Consideration of Non-ground Effect by a Two-Step Deep Learning Inverse Design Method

WANG Chenlu[1], *SUN Jianhong*[1,2,3*], *ZHENG Daren*[1], *SUN Zhi*[2], *ZUO Si*[1], *LIU Hao*[1], *LI Pei*[1]

1. Key Laboratory of Aircraft Environment Control and Life Support, Ministry of Industry and Information Technology, Nanjing University of Aeronautics and Astronautics, Nanjing 210016, P. R. China; 2. Key Laboratory of Civil Aviation Emergency Science & Technology, Civil Aviation Administration of China, Nanjing University of Aeronautics and Astronautics, Nanjing 211106, P. R. China; 3. State Key Laboratory of Mechanics and Control for Aerospace Structures, Nanjing University of Aeronautics and Astronautics, Nanjing 210016, P. R. China

(Received 31 December 2024; revised 8 January 2025; accepted 16 January 2025)

Abstract: Under complex flight conditions, such as obstacle avoidance and extreme sea state, wing-in-ground (WIG) effect aircraft need to ascend to higher altitudes, resulting in the disappearance of the ground effect. A design of high-speed WIG airfoil considering non-ground effect is carried out by a novel two-step inverse airfoil design method that combines conditional generative adversarial network (CGAN) and artificial neural network (ANN). The CGAN model is employed to generate a variety of airfoil designs that satisfy the desired lift-drag ratios in both ground effect and non-ground effect conditions. Subsequently, the ANN model is utilized to forecast aerodynamic parameters of the generated airfoils. The results indicate that the CGAN model contributes to a high accuracy rate for airfoil design and enables the creation of novel airfoil designs. Furthermore, it demonstrates high accuracy in predicting aerodynamic parameters of these airfoils due to the ANN model. This method eliminates the necessity for numerical simulations and experimental testing through the design procedure, showcasing notable efficiency. The analysis of airfoils generated by the CGAN model shows that airfoils exhibiting high lift-drag ratios under both flight conditions typically have cambers of among [0.08c, 0.105c], with the positions of maximum camber occurring among [0.35c, 0.5c] of the chord length, and the leading-edge radiuses of these airfoils primarily cluster among [0.008c, 0.025c].

Key words: conditional generative adversarial network (CGAN); artificial neural network (ANN); airfoil design; wing-in-ground (WIG) aircraft; ground effect

CLC number: V211.4 **Document code:** A **Article ID:** 1005-1120(2025)01-0056-14

0 Introduction

When the wing-in-ground (WIG) effect aircraft operates near the surface of ground or water, the airflow beneath the wings is affected by the ground, causing changes in the aerodynamic characteristics of wings[1]. Unlike the conventional vessel, WIG aircraft maintain no contact with the water during operation, thus eliminating hydrodynamic drag and enabling remarkable increases in cruising speeds over water. Compared to traditional fixed-wing aircraft, WIG aircraft do not rely on runways for take-off and landing, endowing them with exceptional maneuverability and stealth capabilities. The WIG aircraft is highly valuable in areas such as maritime rescue, emergency response, surveillance, and defense[2]. When flying in uneven ground or extreme sea state, WIG aircraft need to operate at elevated altitudes, which results in the loss of ground effect

*Corresponding author, E-mail address: jhsun@nuaa.edu.cn.

How to cite this article: WANG Chenlu, SUN Jianhong, ZHENG Daren, et al. Optimization of high-speed WIG airfoil with consideration of non-ground effect by a two-step deep learning inverse design method[J]. Transactions of Nanjing University of Aeronautics and Astronautics, 2025,42(1):56-69.

http://dx.doi.org/10.16356/j.1005-1120.2025.01.004

and a reduction in the lift-to-drag ratio (L/d)[3]. Consequently, it is essential to develop airfoil designs that are effective in both ground effect and non-ground effect scenarios to ensure the successful operation of WIG aircraft under challenging flying conditions[4].

In recent years, as optimization algorithms have continuously advanced, some researchers have attempted to employ various optimization algorithms in the design of airfoils for WIG aircraft. Lee[5] selected some of the previous Pareto optima for applying to a three-dimensional vehicle with a fuselage, lifting and control surfaces such as a horizontal tail, in order to analyze its aerodynamic characteristics, stability, and three-dimensional effect. He et al.[6] optimized the airfoil NACA 4412 using a multi-objective genetic algorithm, and the lift coefficient and lift-to-drag ratio of the optimized airfoil were significantly improved. Hu et al.[7] used the free deformation technique and artificial neural network method to optimize airfoil shape in ground effect. They obtained an S-shaped airfoil with a maximum lift-drag ratio with satisfying stability. Rejish et al.[8] adopted a parametric shape modeler, a low fidelity solver, and a non-dominated sorting genetic algorithm (NSGA-Ⅱ) to support the preliminary airfoil design of WIG aircraft. Wang et al.[9] used a global aerodynamic optimization method based on the Kriging model to enhance the lift-to-drag ratio for the airfoil design of WIG aircraft across Mach number of 0.2, 0.3, 0.5, and 0.8.

Conventional optimization design methods exhibit inefficiency due to their reliance on iterative numerical simulation analyses. With the development of deep learning, Mirza et al.[10] proposed a conditional generative adversarial network (CGAN), which remedies the existing deficiencies in traditional optimization algorithms. The CGAN was initially widely used in image conversion, feature synthesis, production, editing of artwork and other fields. In 2020, Achour et al.[11] was the first to implement CGAN in the context of airfoil design, successfully generating airfoils that satisfy specified lift-to-drag ratios and surface areas. Wang et al.[12] conducted a comparative analysis of two generative models: the conditional variational autoencoder (CVAE) and an integrated generative network combining CVAE and generative adversarial network (CVAE-GAN). The findings revealed that the CVAE-GAN model significantly outperformed the CVAE model, achieving enhanced reconstruction accuracy across all samples within the dataset. Wu et al.[13] introduced a novel data-augmented GAN (daGAN), which was designed for the swift and precise prediction of flow fields, particularly in scenarios characterized by limited data availability. The findings indicated that daGAN serves as a promising instrument for the rapid and accurate assessment of intricate flow fields, obviating the necessity for extensive training datasets.

CGAN models have demonstrated the capability to generate airfoils that satisfy design specifications. However, the aerodynamic parameters of the generated airfoil necessitate numerical simulation for determination. In response to this issue, a regression prediction model is incorporated subsequently to the CGAN model to facilitate the forecasting of aerodynamic parameters for the generated airfoil. The algorithms of regression prediction can be classified into three categories. The first one contains machine learning algorithms such as linear regression (LR)[14], support vector regression (SVR)[15] or decision trees such as random forest regression (RFR) and stochastic gradient tree boosting (SGTB)[16]. In the second category, deep learning methods like long-short term memory (LSTM), multi-layer perceptron (MLP) and artificial neural network (ANN) are prominent[17]. Lastly, researchers compared surrogate models such as Gaussian process regression (GPR) and proper orthogonal decomposition (POD)[18]. ANN is the basic supervised deep learning method that can be employed to classify and predict the data using labeled datasets, or to train algorithms[19]. Moin et al.[20] proposed a data-driven model to predict aerodynamic coefficients using sparse normalized 2D airfoil coordinates and ANN.

The application of this approach in the realm of aerodynamic design has addressed the limitations of conventional optimization design methods, offering

several advantages. Initially, CGAN enables the generation of airfoil shapes that adhere to specified constraints. The ANN model can predict the aerodynamic parameters of the generated airfoils. Thereby this approach obviates the need for numerical simulations and empirical testing during the design process, significantly reducing the airfoil design cycle duration. In addition, the model has the capability to acquire knowledge of the correlation between the geometric and aerodynamic characteristics of the airfoil, enabling it to produce the necessary airfoil without relying on designer expertise during the design phase. Furthermore, CGAN has the capability to generate a variety of airfoil designs that meet specified constraints, thereby offering designers a broader selection of options.

In this paper, a database for airfoils under near-ground and free-stream conditions at $Ma=0.6$ and $a=6^\circ$ is established. Subsequently, a two-step deep learning design framework based on CGAN and ANN is introduced. After training based on the database, the CGAN is utilized to design airfoils that meet lift-drag ratios under both ground effect and non-ground effect conditions. The lift coefficient (C_l), drag coefficient (C_d), and moment coefficient (C_m) of airfoils designed by CGAN are predicted using the ANN model. In the results discussion section, two models are assessed, and the designed airfoil is examined, considering its geometric and aerodynamic characteristics.

The contributions of our work can be summarized into two aspects. One is to provide a framework for airfoil inverse design under a certain operating condition, which takes advantage of CGAN design model and ANN prediction model, providing reference for the design of airfoil under more states. Secondly, by analyzing the geometric and aerodynamic attributes of the airfoil designed by CGAN model, this paper offers insights for airfoil design of WIG aircraft under challenging flying conditions.

1 Dataset Preparation

The training of CGAN and ANN models require a large amount of sample data. Prior research has predominantly relied on the UIUC database[21] for the reverse design of airfoils. However, the majority of airfoils within this database are low-speed airfoils, rendering them unsuitable for the high-speed airfoil design of WIG aircraft discussed in this study. Consequently, this research opts to utilize the NACA4412 airfoil, a frequently employed airfoil in prior ground effect investigations[22], as the benchmark airfoil for developing a library of high-speed ground effect airfoils. This section provides a comprehensive account of the database creation process and the numerical simulation techniques employed to calculate aerodynamic parameters.

1.1 Establishment of airfoil database

A high-quality database can help the model learn the characteristics of the data better, thus improving the accuracy and effectiveness of the model. To ensure the diversity and availability of the data sets, the class function/shape function transformation (CST) parametrization method[23] and Latin hypercube sampling (LHS) strategy[24] are applied to generate 1 500 airfoils in the design space. The CST parametrization equations are presented as follows

$$y = C(x)\cdot \mathrm{SA}(x) + x\cdot y_{\mathrm{TE}} \tag{1}$$

where y is the y-coordinates of the airfoil, x the x-coordinate, y_{TE} the last y-coordinates of the tailing edge of the airfoil, $C(x)$ the class function, and $\mathrm{SA}(x)$ the shape function of airfoils.

$C(x)$ is presented as

$$C(x) = x^{n_1}\cdot(1-x)^{n_2} \tag{2}$$

where n_1 and n_2 are usually set to 0.5 and 1.0, respectively.

$\mathrm{SA}(x)$ is shown as

$$\mathrm{SA}(x) = \sum_{i=0}^{N} A_i \cdot S_i(x) \tag{3}$$

where A_i are undetermined coefficients and $S_i(x)$ is the Bernstein polynomial defined as

$$S_i(x) = \frac{N!}{i!(N-i)!} x^i (1-x)^{N-i} \tag{4}$$

where N is set to 4.

There are five design parameters allocated to both the upper and lower surfaces, resulting in a combined total of ten design variables. The upper and lower limits for the ten variables are shown as

$$\begin{cases} A_{i\text{up}} = A_{i\text{base}} + 0.1 \\ A_{i\text{low}} = A_{i\text{base}} - 0.1 \end{cases} \tag{5}$$

where $A_{i\text{up}}$ and $A_{i\text{low}}$ are the up and low limits of undetermined coefficients, respectively; $A_{i\text{base}}$ is undetermined coefficients of NACA4412 which are solved using the least-square method and the airfoil coordinates of NACA4412.

By setting thresholds for the ten variables, the database identifies the upper and lower boundaries of the airfoil as illustrated in Fig.1. Subsequently, a total of 1 500 airfoils are produced within this design space utilizing the Latin hypercube sampling shown in Fig.2. Here c denotes the chord length.

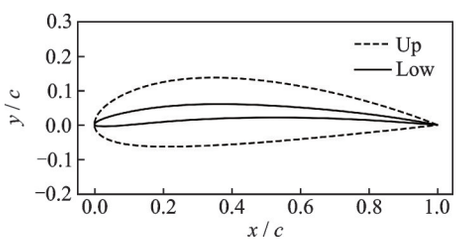

Fig.1 Upper and lower boundaries of airfoil shape in database

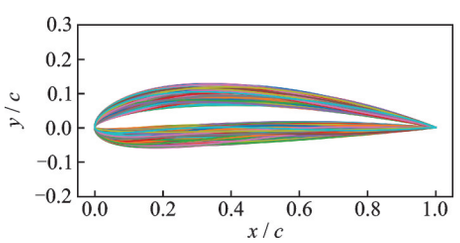

Fig.2 Latin supercube sampled airfoil shapes

1.2 Calculation of aerodynamic parameters

1.2.1 Governing equations and calculation conditions

The RANS method is employed to calculate the aerodynamic parameters of 1 500 airfoils with and without ground effect conditions. The mathematical formulations representing the governing equations are outlined as follows

$$\begin{cases} \dfrac{\partial \rho u_i}{\partial x_i} = 0 \\ \dfrac{\partial (\rho u_i u_j)}{\partial x_j} = -\dfrac{\partial p}{\partial x_i} + \dfrac{\partial \tau_{ij}}{\partial x_j} \\ \dfrac{\partial [(\rho E + p) u_i]}{\partial x_i} = -\dfrac{\partial q_i}{\partial x_i} + \dfrac{\partial (u_j \tau_{ij})}{\partial x_i} \end{cases} \tag{6}$$

where ρ, p, and E represent the density, pressure, and total energy of the fluid, respectively; u_i and u_j represent the velocity component and the component of viscous stress, respectively; q_i represents the heat flux.

The aerodynamic parameters and computational conditions of the airfoil under investigation are as follows in this research.

The lift-drag ratio ($(L/d)_1$), lift coefficient (C_{l1}), drag coefficient (C_{d1}), and moment coefficient (C_{m1}) in ground effect. The calculation conditions are T=288 K, Ma=0.6, h/c=0.2 and a=6°.

The lift-drag ratio ($(L/d)_2$), lift coefficient (C_{l2}), drag coefficient (C_{d2}), and moment coefficient (C_{m2}) in non-ground effect. The calculation conditions are T=288 K, Ma=0.6, h/c=30 and a=6°.

1.2.2 Numerical method validation

In order to evaluate the accuracy of the numerical method for predicting the flow field and aerodynamic forces on an airfoil in ground effect and non-ground effect, the flow fields of a RAE2822 airfoil in two flight conditions are simulated and compared with the wind tunnel experiment data. The diagrams depicting the mesh surrounding the airfoil can be observed in Fig.3[25], with the section close to the airfoil being encrypted and the first layer grid height being $1e^{-5}c$. Fig.4 shows the excellent comparison between the pressure coefficient distribution from numerical simulation and experimental data.[26]

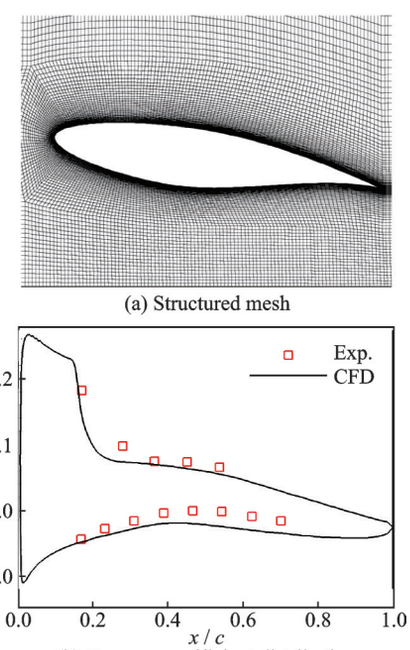

Fig.3 Mesh and comparison of computed and experimental pressure coefficients for the RAE2822 airfoil (h/c=0.23, Ma=0.63, AOA=6°)[25]

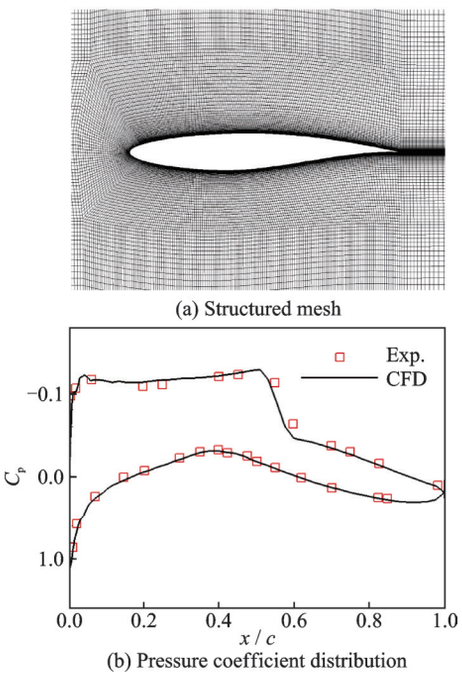

Fig.4 Mesh and comparison of computed and experimental pressure coefficients for the RAE2822 airfoil (Freeflight, Ma= 0.73, AOA=2.3°)[26]

2 Methodology

2.1 Two-step inverse design framework

Following the establishment of the database, airfoils are labeled with different labels based on the L/d range under distinct flight conditions. These labels are subsequently utilized for the training of the CGAN model. The training of the ANN is conducted using C_l, C_d, and C_m. The training process is shown in Fig.5. Following the completion of training, the CGAN model is capable of bypassing the numerical simulation phase and producing numerous airfoil designs that align with specified labels. Subsequently, an ANN model is employed to forecast the aerodynamic parameters of the generated airfoil designs, facilitating the choice of the airfoil based on the projected parameters. The schematic representation of this design procedure is depicted in Fig.6.

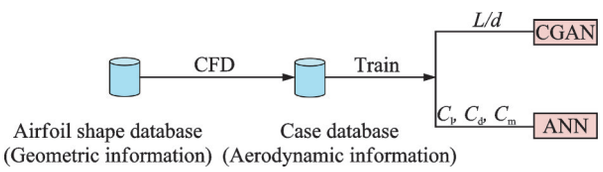

Fig.5 Flow chart of CGAN model and ANN model training

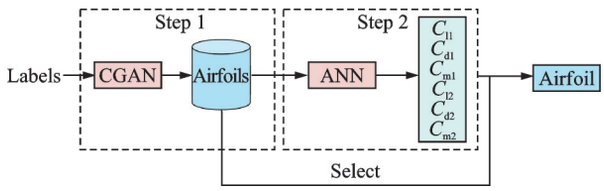

Fig.6 Flow chart of airfoil inverse design

2.2 CGAN design model

2.2.1 Structure of CGAN

Fig.7 illustrates the framework of the CGAN model, comprising a generator (G) and a discriminator (D). The generator and discriminator are designed with opposite training objectives. The generator is responsible for producing airfoil shapes that adhere to conditional information by utilizing random noise and conditional inputs. During the training phase, the network aims to reduce the loss function, shown as

$$L_{\text{generator}} = \log(1 - D(G(z|y))) \tag{7}$$

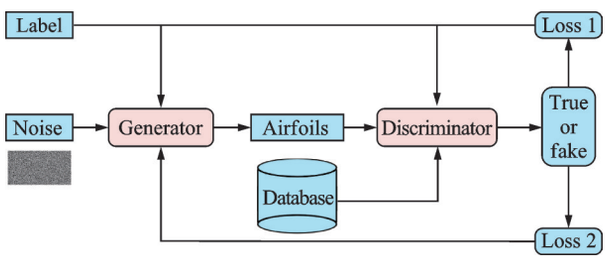

Fig.7 Framework of CGAN

The discriminator distinguishes between real and synthetic airfoil shapes. Throughout the training process, the discriminator is tasked with maximizing the loss functions, shown as

$$L_{\text{discriminator}} = \log(1 - D(G(z|y))) + \log D(x) \tag{8}$$

The loss function used during training is shown as

$$\min_G \max_D V(D,G) = E_{x\sim p_{\text{data}}(x)}[\log D(x|y)] + E_{z\sim p_z(z)}[\log(1 - D(G(z|y)))] \tag{9}$$

As illustrated in Fig.8, the generator and discriminator networks in the CGAN model are built using MLP based on fully connected (FC) layers. An input vector for the generator network is created by combining a conditional vector $\boldsymbol{y}$ with the size of $n\times 1$ and a noise vector $\boldsymbol{z}$ with the size of 100×1.

The generator produces a 120×200×1 three-dimensional matrix showing a grayscale airfoil image. An input layer, three hidden layers, three batch normalization layers, three dropout layers and an output layer make up the generator network. The hidden layer activation functions use LeakyReLU. The generator's detail network parameters are shown in Table 1.

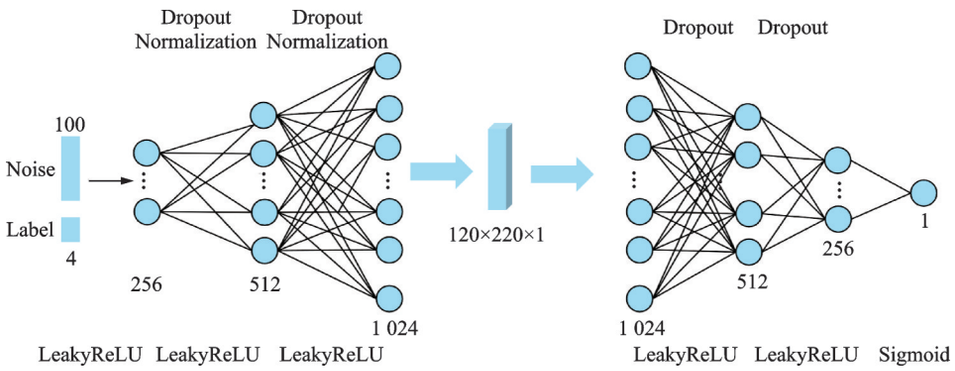

Fig.8 Network structure of generator and discriminator

Table 1 Detailed parameters of generator network

Layer	Input size	Output size	Activation	Dropout layer	Normalization layer
1	104	256	LeakyReLU	√	√
2	256	512	LeakyReLU	√	√
3	512	1 024	LeakyReLU	√	√
4	1 024	120×220×1	Tanh		

The labels and either the airfoil shape image produced by the generator or an actual airfoil shape picture from the airfoil database are received by the generator as input. Its output is a fixed numerical value within the range of 0 to 1, indicating the likelihood that the airfoil originates from the training dataset as opposed to being generated by generator. The discriminator architecture comprises an input layer, three hidden layers, three dropout layers, and an output layer. The activation functions employed in hidden layers and output layers are LeakyReLU and Sigmoid, respectively. The discriminator's detail network parameters are shown in Table 2.

Table 2 Detailed parameters of discriminator network

Layer	Input size	Output size	Activation	Dropout layer	Normalization layer
1	120×220×1	1 024	LeakyReLU	√	—
2	1 024	512	LeakyReLU	√	—
3	512	256	LeakyReLU	√	—
4	128	1	Sigmoid		

2.2.2 Evaluating metrics of CGAN

In this paper, the database serves as the training dataset for the model to optimize the weights and bias parameters. Subsequently, the trained CGAN model is employed to produce airfoils for each label followed by conducting numerical simulations on these airfoils. These generated airfoils are utilized as a validation set to assess the CGAN model's efficacy in airfoil design.

The evaluation of the CGAN's performance is conducted through the utilization of two metrics: accuracy ratio (AR) and distance measure (DM).

The AR signifies the proportion of airfoils within the validation set that conforms to the specified label, serving as a means to assess the CGAN's proficiency in producing accurate airfoils. The AR is expressed as

$$\mathrm{AR}=\frac{m_1}{m} \tag{10}$$

where m represents the number of airfoils generated by CGAN, and m_1 the number of airfoils corresponding to the label after numerical simulation. Here 25 airfoils are generated for each label, so $m=25$.

The DM is used to assess the ability of the CGAN to generate novel airfoil shapes, which is defined as

$$\mathrm{DM}=\min\prod_{j=1}^{1\,500}\left(\sum_{i=1}^{20}\sqrt{(y_i-y_{ji})^2}\right) \tag{11}$$

where y_i is the ith ordinate of the generated airfoil and y_{ji} the ith ordinate of the jth airfoil in the airfoil database.

2.3 ANN prediction model

2.3.1 Structure of ANN

The architecture diagram of the ANN model employed is depicted in Fig.9. The model comprises multiple FC layers. Various hyperparameters of the ANN, such as the quantity of layers, neurons within each layer, epochs, batch size, learning rate, among others, are fine-tuned by exhaustively exploring all feasible combinations of these hyperparameters to identify the most effective configuration for training. It is determined that the optimal performance is achieved when utilizing a two-layer network with 128 neurons in the initial layer and 64 neurons in the subsequent layer. The ideal number of epochs and batch size are determined to be 1 500 and 48, respectively. The activation function employed by the model is Tanh, and the learning rate is set to 0.001. The detailed parameters of the ANN network are shown in Table 3.

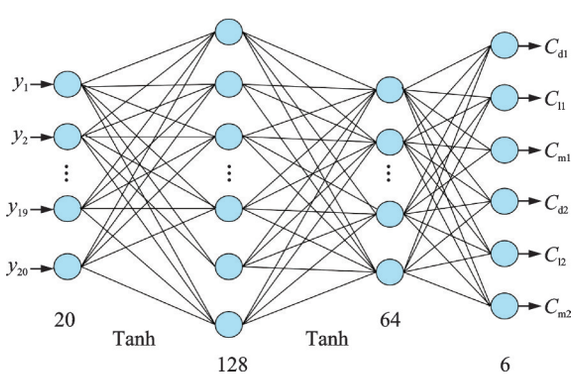

Fig.9 Network structure of ANN

Table 3 Detailed parameters of ANN network

Layer	Input size	Output size	Activation
1	20	128	Tanh
2	128	64	Tanh
3	64	6	

2.3.2 Evaluating metrics of ANN

The experimental design involvs 1 500 airfoils to serve as the training set, while 100 airfoils produced by the CGAN are utilized as the test set to assess the predictive accuracy of the ANN. The aerodynamic parameters of the airfoil anticipated by the ANN model pertain to a regression issue. The standard evaluation metrics for regression problems typically consist of root mean squared error (RMSE), mean absolute error (MAE)[27], and R-squared (R^2)[28].

RMSE is a measure of how spread out these residuals are, and it is usually used to show how concentrated the data is distributed around the line of best fit.

$$\mathrm{RMSE}=\sqrt{\frac{1}{n}\sum_{i=1}^{n}(\hat{y}_i-y_i)^2} \tag{12}$$

MAE is simply calculated as the sum of absolute difference between predicted and actual values divided by the sample size.

$$\mathrm{MAE}=\frac{1}{n}\sum_{i=1}^{n}|\hat{y}_i-y_i| \tag{13}$$

R^2 is the measurement of the range of variation about the best-fit line relative to overall variation in real value. $R^2=1.0$ indicates that the predicted values show the same trend of actual values.

$$R^2=1-\frac{\sum_{i=1}^{n}(y_i-\hat{y}_i)^2}{\sum_{i=1}^{n}(y_i-y^2)^2} \tag{14}$$

where $\hat{y}_i$ and y_i are the predicted and actual values at point i, respectively; and n is the sample size.

3 Results and Discussion

3.1 Training and validation

In the cases with two attributes of $(L/d)_1$ and $(L/d)_2$, four classes can be induced by setting thresholds for each attribute. After being one-hot encoded, the discrete labels will be put into the CGAN

model. The lift-drag ratio intervals for airfoils corresponding to different labels are shown in Table 4.

Table 4 Range of lift-drag ratio for airfoils with different labels

Label	1	2	3	4
$(L/d)_1$	(80,200]	(80,200]	(0,80]	(0,80]
$(L/d)_2$	(40,100]	(0,40]	(40,100]	(0,40]
Code	[1,0,0,0]	[0,1,0,0]	[0,0,1,0]	[0,0,0,1]

Fig.10 illustrates the distributions of aerodynamic parameters for airfoils under two different flight conditions within the dataset. A linear function $y=x$ is represented by the red dashed line, while the black dashed line is utilized to separate four distinct labels. The top figure of the curve shows the variation of aerodynamic parameters in ground effect while the right figure indicates variation of aerodynamic parameters in non-ground effect. The middle figure of the contour line represents the probability density. The middle figure of the L/d and C_l are all situated below the line $y=x$, whereas that of the C_d is positioned above it. This distribution characteristics indicate that the ground effect yields to an increased lift and reduced drag, as well as the increased lift-drag ratio. The analysis of the C_m distribution reveals a direct correlation between the C_m values of the airfoils under two different flight conditions. Furthermore, the ground effect is noted to increase C_m, resulting in a reduction in the pitch stability of the airfoils. Evidently seen from separate $(L/d)_1$ and $(L/d)_2$ variation curves, the values of $(L/d)_1$ are mainly distributed among [20, 120], while the $(L/d)_2$ are mainly distributed among [10, 60]. From the combined distribution of $(L/d)_1$ and $(L/d)_2$, it can be seen that $(L/d)_1$ and $(L/d)_2$ are concentrated around values of 45 and 20, respectively.

The time required for CGAN to generate an airfoil design is 1.2 s, while ANN model takes 0.4 s to predict aerodynamic parameters. Consequently, this inverse design framework enables an airfoil design meeting specified criteria and the acquisition of its aerodynamic characteristics within a total time of

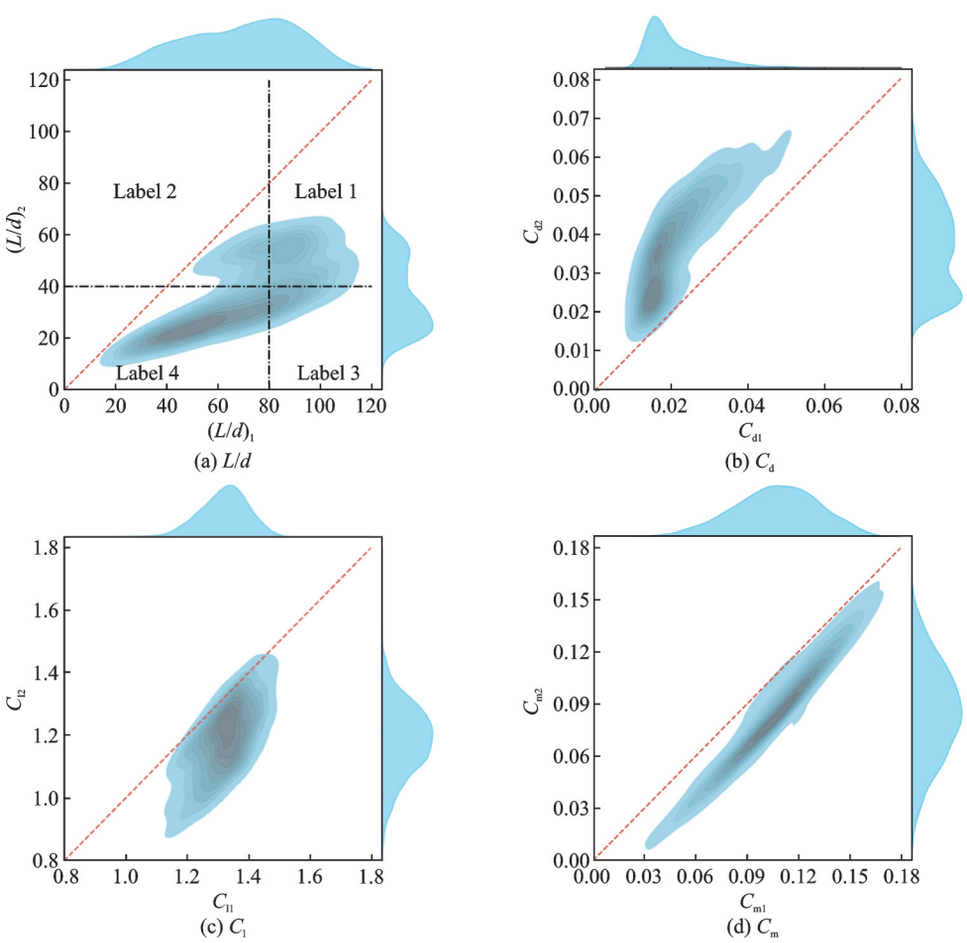

Fig.10 Aerodynamic parameter distribution of airfoils under two different flight conditions

1.6 s. In order to evaluate the time performance, a CFD simulation is carried out on the same desktop, requiring approximately 1 800 s for convergence to be achieved. The reverse design approach outlined in this research significantly reduces the time required by nearly 1 000 times in comparison to CFD, highlighting substantial time-saving benefits.

The accuracy rate of the CGAN model for different labels are shown in Fig.11. The model achieves the highest design accuracy rate for airfoils labeled as 4, with Label 1 airfoils closely trailing behind in accuracy. Conversely, airfoils labeled as 2 and 3 exhibit the lowest design accuracy rates. There is a positive correlation between the quantity of airfoils categorized under various labels and the accuracy rate of the model. This suggests that augmenting the training dataset size can lead to enhancements in model accuracy. Fig.12 illustrates the proportion of correct and incorrect airfoils generated by CGAN when focused on different flight conditions. The CGAN demonstrates a commendable accuracy rate of 82% when takeing both $(L/d)_1$ and $(L/d)_2$ into consideration, suggesting its reliability. Furthermore, Fig.12(b) presents the accuracy rates of CGAN when solely focusing on $(L/d)_1$ with accuracy rate of 88% which is lower than the accuracy rate of 93% observed in Fig.12(c) when concentrating on $(L/d)_2$. The increased intricacy of the airfoil's

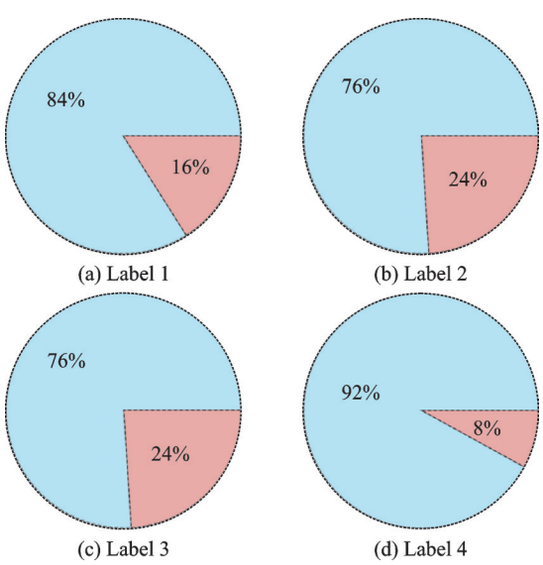

Fig.11 Pie chart of the proportion for correct and incorrect airfoils generated by CGAN when focused on different labels

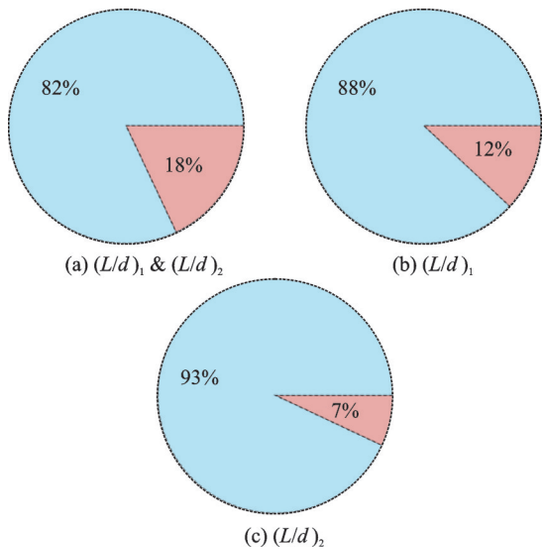

Fig.12 Pie chart of the proportion for correct and incorrect airfoils generated by CGAN with and without ground effect conditions

aerodynamic characteristics influenced by ground effect leads to the struggle to effectively assimilate of the model.

The distance measurements between the generated and original airfoils are shown in Fig.13. The dashed red lines separate the DM distribution of different labels. It is observed that all distance matrices exceed a value of 0.575, with a significant proportion of them surpassing 0.7, indicating that the model exhibits the ability to generate novel airfoil shapes. The dataset comprises a greater number of airfoils categorized as Label 4, accompanied by distance matrices that demonstrate elevated values in comparison to the remaining three labels. This finding suggests that an expanded dataset has the capability to enhance the model's ability for generalization.

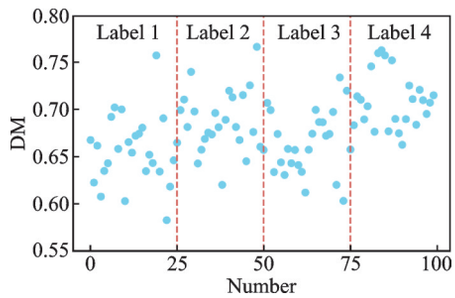

Fig.13 Distribution of distance measurements between generated airfoils and original airfoils in database

Fig.14 shows the evolution of the loss function of ANN versus the number of epochs. The training and testing errors converge after 1 000 epochs. The

performance of the trained model on the testing datasets is comparable to that on the training datasets, showing the generalization of the proposed model. After training, the model is employed to predict new values and validate its performance. Table 5 shows the performance metrics for the ANN model. The R^2 metrics for C_{d1}, C_{d2}, C_{m1} and C_{m2} all exceed 0.9, while that for C_{l1} and C_{l2} is approximately 0.84, which shows reasonable accuracy values for the ANN model. The RMSE are 0.002 63, 0.039, and 0.005 2 for C_{d1}, C_{l1}, and C_{m1}, respectively, and 0.001 78, 0.028, and 0.005 7 for C_{d2}, C_{l2}, and C_{m2}, respectively. Fig.15 shows the scatter plot of the predicted C_l, C_d, and C_m values against their corresponding truth values using the test dataset. Ideally, the scatter points should be on the top of the regressed diagonal line with a slope equal to one, representing a perfect fit. The red dashed line in the diagram represents a 10% error line. It can be seen that most of the predicted results fall within a 10% margin of error, asserting the reliability of the ANN predictions.

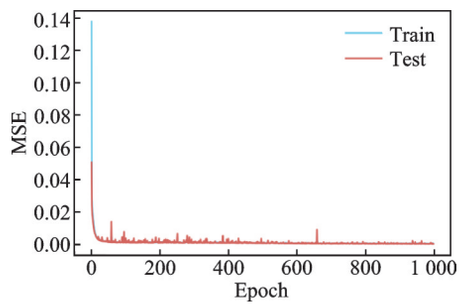

Fig.14 Evolution of loss function of the ANN

Table 5 Performance metrics for the ANN model

Evaluation metric	C_{d1}	C_{l1}	C_{m1}	C_{d2}	C_{l2}	C_{m2}
R_2	0.933	0.840	0.943	0.916	0.842	0.907
RMSE	0.002 63	0.039	0.005 2	0.001 78	0.028	0.005 7
MAE	0.002	0.031	0.004 3	0.001 24	0.019 3	0.004 52

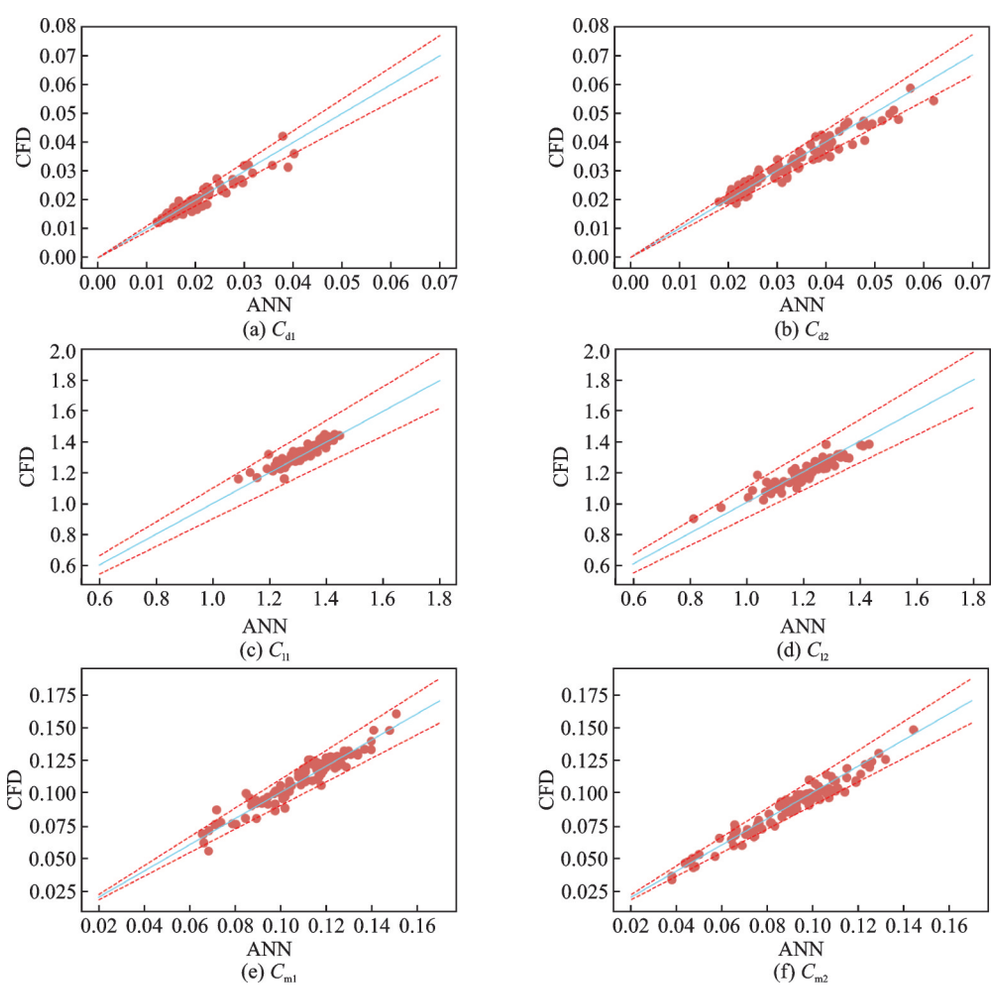

Fig.15 Scatter plots of the predicted C_d, C_l, and C_m versus the corresponding truth values

3.2 Analysis of design airfoils

Then a detailed analysis of the geometric and aerodynamic features of the airfoil designed by CGAN is conducted. The airfoil shapes generated by CGAN with different labels are shown in Fig.16. The blue curves represent airfoils that are excluded from the analysis as they are generated incorrectly. To more intuitively illustrate the differences in geometric features of airfoils corresponding to various labels, Fig.17 illustrates histograms for three key parameters: maximum camber, position of the maximum camber, and leading-edge radius of airfoils. The airfoils labeled as 1 demonstrate excellent aerodynamic performance in both flight conditions. The camber distribution of these airfoils is primarily among $[0.08c, 0.105c]$, with the maximum camber located at approximately among $[0.35c, 0.5c]$. Additionally, the leading-edge radii of airfoils are predominantly situated at around distributed among

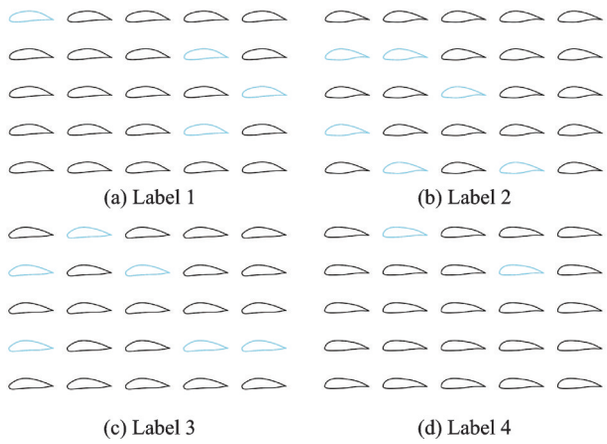

Fig.16 Airfoils of different labels generated by CGAN

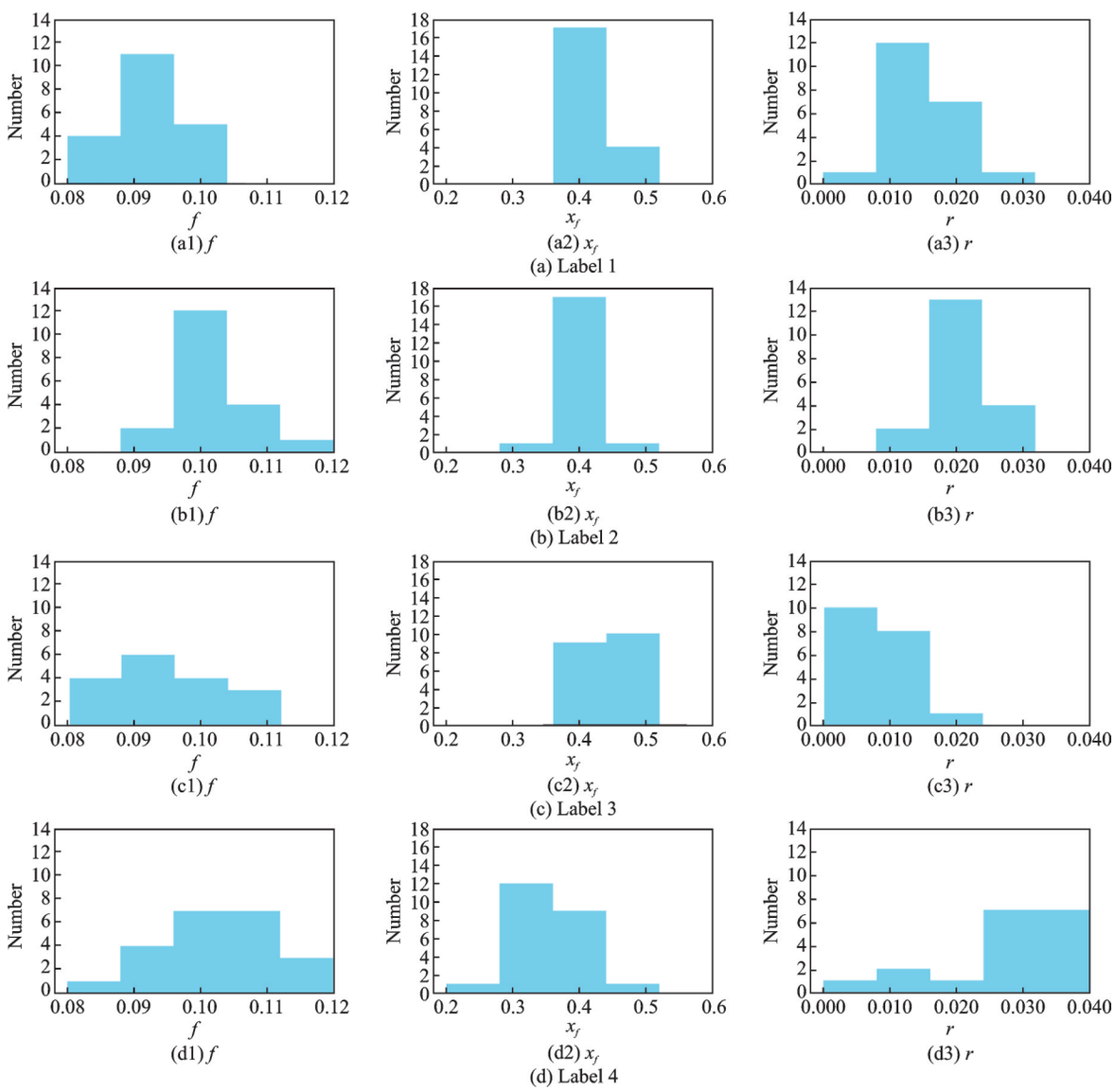

Fig.17 Histograms of geometric parameters for airfoils of different labels

[0.008c, 0.025c]. In comparison to the airfoils identified as Label 1, those labeled as 2 exhibit increased leading-edge radii and cambers. These airfoils may demonstrate decreased lift-drag ratios when flight in ground effect, while maintaining higher lift-drag ratios in non-ground effect. The airfoils identified as Label 3 are characterized by their reduced leading-edge radii, leading to lower lift-drag ratios in non-ground effect conditions and favorable aerodynamic performance in ground effect. Label 4 airfoils are characterized by larger leading-edge radii and forward positions of the maximum camber, leading to reduced lift-drag ratios across both flight conditions.

4 Conclusions

An inverse design of high-speed ground effect airfoil based on a two-step inverse design framework is carried out with the consideration of non-ground effect. A database is developed for the purpose of examining airfoils under various conditions, including near-ground and free-stream scenarios. Subsequently, the data from this database is used to train CGAN and ANN. Next, we evaluate the models and analyze the designed airfoils from both geometric and aerodynamic features. The conclusion can be drawn as follows.

(1) The CGAN model boasts an 82% accuracy rate, attesting to its reliability. The distance matrices for generated airfoils exceed 0.57, affirming the model's capability to produce novel airfoils. The RMSE of ANN for aerodynamic parameters prediction is mostly within 10%, which means the model has the generalization ability to make credible predictions.

(2) By incorporating an ANN model following the CGAN model, it is possible to realize the multi-objective parameter design of airfoils without the need or numerical simulations as well as the experience of designers. This approach significantly enhances the efficiency of airfoil design processes.

(3) The airfoils exhibiting favorable aerodynamic performance in both flight conditions demonstrate concentrated cambers among [0.08c, 0.105c], with the maximum camber positions among [0.35c, 0.5c]. Additionally, the leading-edge radii of these airfoils are primarily centered approximately among [0.008c, 0.025c].

References

[1] HALLORAN M, O'MEARA S. Wing in ground effect craft review[M]. Australia: DSTO Aeronautical and Maritime Research Laboratory, 1999.

[2] SUN J H, WANG C L, ZHENG D R, et al. The future and technique challenges of high-speed ground effect vehicle enrolled in maritime transportation[J]. Aerospace Traffic and Safety, 2024, 1(1): 43-54.

[3] LIU H, SUN J H, ZHENG D R, et al. Numerical simulation and dynamic mode decomposition analysis of the flow past wings with spanwise waviness[J]. Engineering Applications of Computational Fluid Mechanics, 2022, 16(1): 1849-1865.

[4] LIU Hao, SUN Jianhong, SUN Zhi, et al. Circulation control of airfoil aerodynamic force under ground effect of wavy wall[J]. Journal of Shanghai Jiaotong University, 2022, 56(8): 1101-1110. (in Chinese)

[5] LEE J. Computational analysis of static height stability and aerodynamics of vehicles with a fuselage, wing and tail in ground effect[J]. Ocean Engineering, 2018, 168: 12-22.

[6] HE Y, QU Q, AGARWAL R K. Shape optimization of an airfoil in ground effect for application to WIG craft[J]. Journal of Aerodynamics, 2014(1): 931232.

[7] HU H, ZHANG G, LI D, et al. Shape optimization of airfoil in ground effect based on free-form deformation utilizing sensitivity analysis and surrogate model of artificial neural network[J]. Ocean Engineering, 2022, 257: 111514.

[8] REJISH J, RAFFAELLO M, ARDESHIR H. Preliminary aerodynamic wing design optimization for wing-in-ground effect aircraft [C]//Proceedings of 2017 International Conference on Evolutionary and Deterministic Methods for Design Optimization and Control with Application to Industrial and Societal Problems (EUROGEN). Stockholm, Sweden: Springer, 2017: 1-10.

[9] WANG Chenlu, SUN Jianhong, SUN Zhi, et al. Optimization of lift-to-drag characteristics for high-speed wing-in-ground effect based on the kriging model[J]. Journal of Aerospace Power, 2024. DOI: 10.13224/j.cnki.jasp.20230550.

[10] MIRZA M, OSINDERO S. Conditional generative adversarial nets[EB/OL]. (2024-10-01). https://doi.

org/10.48550/arXiv.1411.1784.

[11] ACHOUR G, SUNG W J, PINON-FISCHER O J, et al. Development of a conditional generative adversarial network for airfoil shape optimization[C]//Proceedings of AIAA Scitech 2020 Forum. Orlando, USA: AIAA, 2020.

[12] WANG J, RUNZE L I, CHENG H E, et al. An inverse design method for supercritical airfoil based on conditional generative models[J]. Chinese Journal of Aeronautics, 2022, 35(3): 62-74.

[13] WU H Z, LIU X J, WEI A N, et al. A generative deep learning framework for airfoil flow field prediction with sparse data[J]. Chinese Journal of Aeronautics, 2022, 35(1): 470-484.

[14] ANDRÉS P E, PAULETE P C. On the application of surrogate regression models for aerodynamic coefficient prediction[J]. Complex & Intelligent Systems, 2021, 7: 1991-2021.

[15] CHEN S L, GAO Z H, ZHU X Q, et al. Unstable unsteady aerodynamic modeling based on least squares support vector machines with general excitation[J]. Chinese Journal of Aeronautics, 2020, 33(10): 2499-2509.

[16] NAGAWKAR J, LEIFSSON L. Multifidelity aerodynamic flow field prediction using random forest-based machine learning[J]. Aerospace Science and Technology, 2022, 123: 107449.

[17] HU L, ZHANG J, XIANG Y, et al. Neural networks-based aerodynamic data modeling: A comprehensive review[J]. IEEE Access, 2020, 8: 90805-90823.

[18] SABATER C, STÜRMER P, BEKEMEYER P, et al. Fast predictions of aircraft aerodynamics using deep-learning techniques[J]. AIAA Journal, 2022, 60(9): 1-13.

[19] YETKIN S, ABUHANIEH S, YIGIT S, et al. Investigation on the abilities of different artificial intelligence methods to predict the aerodynamic coefficients[J]. Expert Systems with Applications, 2024, 237: 121324.

[20] MOIN H, KHAN H Z I, MOBEEN S, et al. Airfoil's aerodynamic coefficients prediction using artificial neural network[C]//Proceedings of the 19th International Bhurban Conference on Applied Sciences and Technology (IBCAST2022). Islamabad, Pakistan: [s.n.], 2022.

[21] SELIG M S. UIUC airfoil data site[EB/OL]. 1996, https://m-selig.ae.illinois.edu/ads.html.

[22] LEE J, HAN C S, BAE C H. Influence of wing configurations on aerodynamic characteristics of wings in ground effect[J]. Journal of Aircraft, 2010, 47(3): 1030-1040.

[23] KULFAN B, BUSSOLETTI J. "Fundamental" parameteric geometry representations for aircraft component shapes[C]//Proceedings of the 11th AIAA/ISSMO Multidisciplinary Analysis and Optimization Conference. Portsmouth, UK: AIAA, 2006.

[24] SHIELDS M D, ZHANG J. The generalization of Latin hypercube sampling[J]. Reliability Engineering & System Safety, 2016, 148: 96-108.

[25] DOIG G, BARBER T J, NEELY A J, et al. Aerodynamics of an aerofoil in transonic ground effect: Methods for blowdown wind tunnel scale testing[J]. Journal of Aeronautics, 2012, 116(1180): 599-620.

[26] BAI W. Analyses of wind-tunnel test data of the transonic airfoil RAE2822[J]. Acta Aerodynamica Sinica, 2023, 41(6): 55-70.

[27] WILLMOTT C J, MATSUURA K. Advantages of the mean absolute error (MAE) over the root mean square error (RMSE) in assessing average model performance[J]. Climate Research, 2005, 30(1): 79-82.

[28] PECK R, OLSEN C, DEVORE J L. Introduction to statistics and data analysis[M]. Stamford: Cengage Learning, 2016: 11-13.

Acknowledgements This work was supported by the Priority Academic Program Development of Jiangsu Higher Education Institutions, the Fundamental Research Funds for the Central Universities (No.ILA220101A23), CARDC Fundamental and Frontier Technology Research Fund (No. PJD20200210), and the Aeronautical Science Foundation of China (No.20200023052002).

Authors

The first author Ms. **WANG Chenlu** received her M.S. degree in Aeronautical and Astronautical Science and Technology from Nanjing University of Aeronautics and Astronautics (NUAA). Her work focuses on efficient surrogate modeling and physics-informed algorithms for sustainable engineering solutions.

The corresponding author Prof. **SUN Jianhong** received his Ph. D. degree in Mechanical Engineering from Hong Kong University of Science and Technology, and has been a Professor and Doctoral Supervisor at NUAA since 2008. His research field is aircraft design, airworthiness technologies, and aviation safety systems, among others.

Author contributions Ms. **WANG Chenlu** conceived the numerical simulation framework, implemented computa-

tional models and wrote the manuscript. Prof. **SUN Jianhong** conceptualized the research objectives, supervised methodological validity, refined theoretical interpretations, and revised the manuscript critically. Dr. **ZHENG Daren** developed high-performance computing algorithms, and co-designed validation workflows. Dr. **SUN Zhi** aggregated experimental datasets and performed statistical benchmarking. Mr. **ZUO Si** conducted systematic literature reviews and contributed to technical discourse. Mr. **LIU Hao** executed sensitivity analyses and resolved model calibration conflicts. Ms. **LI Pei** formalized multiphase coupling mechanisms, interpreted industry-relevant case studies, and co-wrote application sections. All authors commented on the manuscript draft and approved the submission.

Competing interests The authors declare no competing interests.

(Production Editor: WANG Jing)

基于两步深度学习逆向设计方法考虑非地面效应的高速地效翼型优化

王晨鹭[1], 孙建红[1,2,3], 郑达仁[1], 孙 智[2], 左 思[1], 刘 浩[1], 李 佩[1]

(1.南京航空航天大学飞行器环境控制与生命保障工业和信息化部重点实验室,南京 210016,中国;
2.南京航空航天大学民航应急科学与技术重点实验室,南京 211106,中国;
3.南京航空航天大学航空航天结构力学及控制全国重点实验室,南京 210016,中国)

摘要:在避障、极端海况等复杂飞行工况下,地效飞行器需爬升至更高空域,导致地面效应消失。本文通过一种融合条件生成对抗网络(Conditional generative adversarial network, CGAN)与人工神经网络(Artificial neural network, ANN)的新型两步逆向翼型设计方法,开展了考虑非地效工况下的高速地效翼型设计研究。CGAN模型用于生成同时满足地效与非地效工况目标升阻比的多样化翼型设计,ANN模型用于预测生成翼型的气动参数。结果表明,CGAN模型能够生成满足条件的新型构型的翼型,ANN模型对翼型气动参数的预测具有较高精度,该方法在设计过程中无需依赖数值模拟与实验测试,具有显著的高效性。对CGAN生成翼型的分析表明,双工况下具有高升阻比的翼型弯度多分布于[0.08c, 0.105c]区间,最大弯度位置位于弦长的[0.35c, 0.5c]区间,且翼型前缘半径主要集中在[0.008c, 0.025c]范围。

关键词:条件生成对抗网络;人工神经网络;翼型设计;地效翼飞行器;地面效应